NCC1-25

LANGLEY
GRANT
IN-47-CR
319628
P.44

MARYLAND

COLLEGE PARK CAMPUS

PROGRESS OF RESEARCH ON WATER VAPOR LIDAR

by

T. D. Wilkerson
Atmospheric Lidar Observatory
Institute for Physical Science and Technology
University of Maryland, College Park, MD 20742-2431
(301) 405-4850

BN-1120

November 1990

INSTITUTE FOR PHYSICAL SCIENCE AND TECHNOLOGY

(NASA-CR-187673) PROGRESS OF RESEARCH ON WATER VAPOR LIDAR Report, period ending 31 Jul. 1990 (Maryland Univ.) 44 p CSCL 04B

N91-13837

Unclas

G3/47 0319628

PROGRESS OF RESEARCH ON WATER VAPOR LIDAR[1]

by

T. D. Wilkerson
Atmospheric Lidar Observatory
Institute for Physical Science and Technology
University of Maryland, College Park, MD 20742-2431

ABSTRACT

Research is described on several aspects of stimulated Raman scattering (SRS) of 532 nm laser light in H_2, D_2, and CH_4. The goals of this work are: (1) to develop a more thorough understanding of nonlinear processes involving the Raman effect and four-wave mixing, and (2) to find the best way to generate radiation at several wavelengths simultaneously, for lidar applications. Issues addressed are conversion efficiency, optimization of operating conditions (gas pressure, confocal parameter, etc.) and the distribution of output pulse energy over three Stokes components, the first anti-Stokes component, and the zeroth order (pump) wavelength. The described research and results constitute another step in the development of SRS applications for NASA's atmospheric lidar program.

[1]*A report on research carried out under NCC 1-25 (E. V. Browell, Technical Monitor), sponsored by NASA-Langley Research Center, for the period ending July 31, 1990.*

PROGRESS OF RESEARCH ON WATER VAPOR LIDAR

We report on the further study of stimulated Raman scattering (SRS) processes being conducted in College Park. As this program continues, a clearer picture emerges of the possibilities for SRS in atmospheric lidar applications. As a result, we are now able to carry out spectroscopy experiments, for example, at infrared wavelengths that were previously not accessible to most tunable lasers. This latter work, and plans for improved optical conversion efficiency into the near infrared, will be reported in the near future. These developments will have been made feasible, in part, by the research reported in the present document, because of the deeper understanding provided about SRS processes in general.

The work we report here was carried out until May 30, 1990, first submitted as a journal article to *Applied Optics* in August, 1980, and described at two conferences during 1990. (See Appendices A and B.) Appendix C contains the final version of the paper which will be published in *Applied Optics*.

The research consists of an in-depth study of a variety of SRS processes in H_2, D_2, and CH_4 for the input wavelength 532 nm (Nd:YAG,SHG). While this wavelength is intermediate between the near UV wavelengths of interest for ozone lidar specialists and the near IR region for meteorological lidar, it provided us ample energy to:

- Vary the experimental parameters over a wide range;
- Make quantitative observations on Raman components, in addition to the most prominent one (first Stokes); and
- Distinguish in some cases the roles of SRS and four-wave mixing.

Just by itself the latter is important for knowledgeable lidar applications that need to go beyond the simple issue of energy conversion efficiency, to address beam divergence, multiple Stokes interference, and spectral distribution of the output.

Results of this work are described in detail in the submitted article which appears here in Appendix C. The conclusions are reiterated here:

> We have investigated the performance of a single-pass, multi-order Stokes generation system using hydrogen, deuterium and methane gases as Raman media. Among the three gases, CH_4 transfers very little energy to high order Stokes and anti-Stokes outputs; most of the energy is concentrated in the pump and first Stokes, especially at high pressures. Thus CH_4 is appropriate for generating first Stokes light, but not for multiple wavelength applications. For H_2 and D_2, energy is distributed over second Stokes as well as the first Stokes and the transmitted pump. Varying the hydrogen pressure in the range of 5 to 15 atm, and deuterium above 40 atm, is a suitable method for simultaneous generation of a variety of wavelengths with reasonable energy for lidar applications. D_2 is a suitable gas for producing radiation on the shorter wavelength side, and the optimum pressure for this is about 13 atm.

During the reporting period, presentations were made on research carried out under the Cooperative Agreement. Abstracts for these conference proceedings are reproduced in Appendices A and B. This completes our report on NCC 1-25 for the period ending July 31, 1990.

APPENDICES

Appendix A: "Optimization of SRS Techniques for Remote Sensing Applications," U. N. Singh, Z. Chu, and T. D. Wilkerson, *Proc. Conf. on Laser and Electro-Optics (CLEO '90)*, Anaheim, CA (May 21-25, 1990).

Appendix B: "Multiple Wavelength Generation by SRS Technique for Aerosol Measurement," Z. Chu, U. N. Singh, and T. D. Wilkerson, *Proc. 15th Annual Internat'l. Laser Radar Conf.*, Tomsk, U.S.S.R (July 23-27, 1990).

Appendix C: "Multiple Wavelength Generation in Molecular Gases for Lidar Applications," Z. Chu, U. N. Singh, and T. D. Wilkerson, *Applied Optics*, 25 pages, submitted (August, 1990).

APPENDIX A

OPTIMIZATION OF SRS TECHNIQUES FOR REMOTE SENSING APPLICATIONS

U. N. SINGH, Z. CHU, and T. D. WILKERSON

Atmospheric Lidar Observatory
Institute for Physical Science and Technology
University of Maryland, College Park, MD 20742-2431

Telphone: (301) 454-4760

FAX: (301) 454-6062

ABSTRACT

We describe the optimization of the SRS techniques for efficiently generating eye-safe radiation in the near-IR, and multiwavelength radiation in visible and near-IR, for atmospheric aerosol measurements. The optimized results demonstrate the applicability of the SRS process.

OPTIMIZATION OF SRS TECHNIQUES FOR

REMOTE SENSING APPLICATIONS

U. N. SINGH, Z. CHU, and T. D. WILKERSON

Atmospheric Lidar Observatory
Institute for Physical Science and Technology
University of Maryland, College Park, MD 20742-2431

Telphone: (301) 454-4760
FAX: (301) 454-6062

SUMMARY

This paper describes a specific new technique for optimizing a Raman-shifted Nd:YAG laser system capable of generating 1.54 μm radiation in the eye-safe infrared for cloud and aerosol studies. The existing lidar systems are not eye-safe, in general, and pose potential risk of eye damage especially in the case of downward pointing lidar systems. This laser system can also be used to generate multiple wavelengths through SRS (stimulated Raman scattering) to study the aerosol, whose sizes cover many order of magnitude and whose scattering properties strongly depend on the incident wavelength.[1]

The experimental setup used for the studies reported here is shown in Fig. 1. Eye-safe radiation at the first Stokes wavelength of 1.54 μm is produced in the lower Raman cell when methane is used as Raman-active medium, the pump source being a Nd:YAG laser at 1.064 μm. The technique used in this study for optimizing the first Stokes generation involved retroreflecting the backward-generated first Stokes light back into the Raman cell as a seed Stokes beam which was then amplified in the temporal tail of the pump beam We will also discuss the optimization procedures and the limitations.

The advantages of using a seeded amplifier are quite evident in Fig. 2. Compared to the single pass self-generated SRS system , the energy conversion efficiency with this new method tripled and approached 18% at a pressure of 14 atm and a pump energy of 140 mJ at 10 Hz.[2] The conversion efficiency was further improved by operating the system at lower repetition rate (e.g., 5 or 3 Hz). This SRS configuration is currently being used in a flight experiment on a NASA DC-8 aircraft to carry out aerosol lidar measurements as part of the GLObal Backscattering Experiment (GLOBE) project.

Multiwavelength generation by the SRS technique in different molecular gases (H_2, D_2, and CH_4) was studied using a frequency-doubled Nd:YAG laser at 532 nm as the pump source. The Raman cell on the top of Fig. 1 was used, where H_2 has been shown, for example, as a Raman-active medium. The study was focused on the redistribution of the pump energy primarily into four SRS components: fundamental, first Stokes, second Stokes, and first anti-Stokes. The pump energy was varied from 0-200 mJ and the gas pressure from 0-45 atm. Results indicated that among the three gases, CH_4 transfers very little energy to higher order Stokes and anti-Stokes radiation, and most of the energy is found in the undepleted pump and first Stokes, at high cell pressure. Thus it is appropriate for generating first Stokes but not suitable for multiwavelength purposes. For H_2 and D_2, pump energy is fairly well distributed in fundamental, first, and second Stokes. Keeping the hydrogen pressure in the range of 10-20 atm and deuterium above 40 atm, multiwavelength output can be generated with reasonable energy per pulse for aerosol lidar applications.

REFERENCE

1. R.M. Measures, Laser Remote Sensing (John Wiley & Sons, New York, 1984).

2. Z. Chu, U.N. Singh, and T.D. Wilkerson, "A Self-Seeded SRS System for the Generation of 1.54 μm Eye-Safe Radiation", Optics Communications, in press (1990)

FIGURE CAPTIONS

Fig. 1. Experimental arrangement for generating multiwavelength and eye-safe radiation.

Fig.2 Conversion efficiency of the amplified Stokes output(●) is shown as a function of pump energy for a methane gas pressure of 14 atm. For comparison, the conversion efficiency of the backward-generated Stokes seed (O) and the forward Stokes in the unseeded case (■)are also shown.

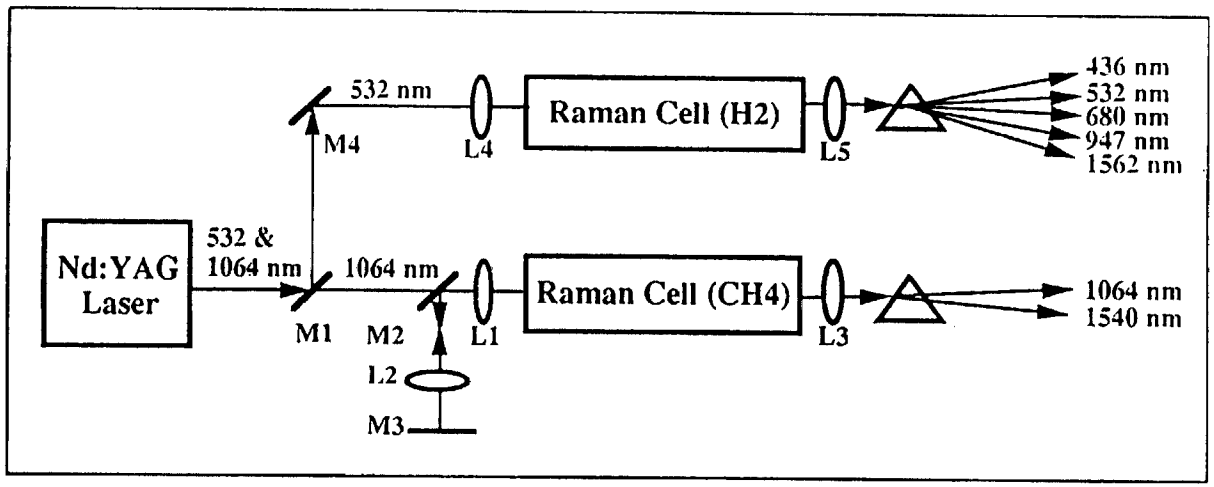

Chu, Singh & Wilkerson

Figure 1.

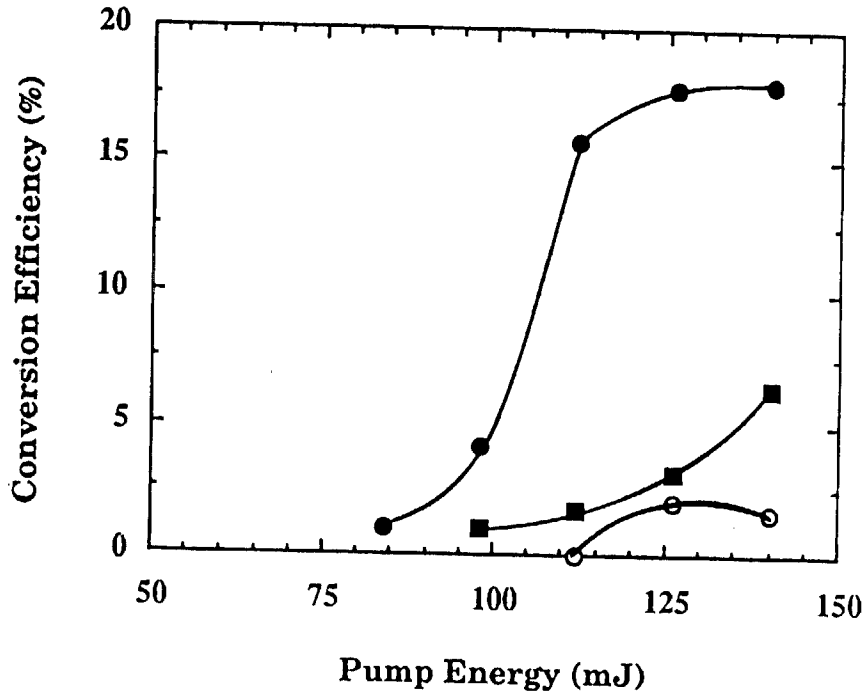

Chu, Singh & Wilkerson

Figure 2.

APPENDIX B

MULTIPLE WAVELENGTH GENERATION BY SRS TECHNIQUE FOR AEROSOL MEASUREMENT

Z. CHU, U. N. SINGH, T. D. WILKERSON

University of Maryland
Institute for Physical Science and Technology
College Park, MD 20742-2431, USA

The atmosphere contains particles whose size distribution cover many orders of magnitude. Because the scattering properties of aerosol strongly depend on the incident wavelength [1], size distribution measurements require radiation at different wavelengths with reasonable energy [2]. Stimulated Raman scattering (SRS) is attractive for this purpose as its multiple Stokes shifts can provide radiations with considerable wavelength difference and reasonable energy.

Multiwavelength generation by SRS in different molecular gases (H_2, D_2 and CH_4) was studied using a frequency-doubled Nd:YAG laser at 532 nm as the pump source. The experimental setup is shown in Fig. 1. A single-pass Raman cell of one meter length was used . The study was focused on the redistribution of the pump energy primarily into four SRS components: fundamental S_0, first Stokes S_1, second Stokes S_2, and first anti-Stokes AS_1. The other higher order radiations were too weak to be considered for lidar applications and were thus neglected. The pump energy was varied from 0-200 mJ and the gas pressure from 0-45 atm. For optimization purposes, we also varied the pump power density at the center of Raman cell by using different focusing geometry. Stimulated Raman scattering characteristics for different gases are discussed and are compared for the purpose of multiple wavelength generation.

Figure 2 shows the energy conversion efficiency of the pump laser to S_0, S_1, S_2 and AS_1 for a range of pump energy in H_2, D_2 and CH_4 at pressure of 20 atm. To compare these results, the Raman gains in H_2, D_2 and CH_4 at pressure of 20 atm were predicted theoretically to be 2.72, 0.56 and 0.63 cm/GW, respectively. It can be seen that Raman gain values in H_2 are much larger than in D_2 and CH_4; the same trend prevails in our measurements shown in Figure 2. The minimum residual pump energy (smallest S_0) in H_2 corresponds to a largest Raman gain, while the maximum residual pump energy (largest S_0) in D_2 corresponds to a smallest Raman gain with an intermediate value for CH_4.

Higher Raman gain in H_2 also supports a strong competition between S_1 and S_2, as evident in Fig. 2 (a). As soon as the pump laser energy exceeded the threshold level, both first Stokes (S_1) and second Stokes (S_2) energies rose rapidly. Each reached an energy conversion efficiency of 30% for a pump energy of 100 mJ. Second Stokes light was generated by cascade SRS excitation and four wave mixing. When the pump energy was increased further, the second Stokes conversion efficiency reached saturation while the first Stokes efficiency showed a slow decrease. Lower gain in D_2 supports a more uniform distribution of pump energy among S_0, S_1, S_2 and AS_1, as seen in Fig. 2 (b). In the saturation regime S_0 is about 38%, S_1 is 22%, S_2 is 12% and AS_1 is 5%. In CH_4, most of the scattered pump photons were converted to S_1. The highest first Stokes energy conversion efficiency with lowest second Stokes indicates that in contrast to H_2 and D_2, four wave mixing is not predominant in compressed CH_4 at 20 atm.

Figure 3 shows the SRS conversion efficiencies as a function of gas pressure (H_2, D_2 and CH_4) for a pump energy of 150 mJ. Two important features are seen with SRS in H_2 (Fig. 3 (a)): (1) an almost constant residual pump energy S_0 in the pressure range of 15 to 50 atm, and (2) the appearance of a minimum in S_1 around 10 atm and a maximum in S_2 near 13 atm. The growth and competing behavior of S_1 and S_2 in low and high pressure regimes are directly related to their generation principle. In the low pressure regime, both the cascade SRS [3] and the four wave mixing effect [4] contribute to S_2 generation. Second Stokes suppression at high pressure is a result of the four wave mixing effect, since Raman gain is independent of pressure, and cascade SRS does not transfer the second Stokes photon to third Stokes radiation, as is evident from the decreasing trend of S_3 with pressure in Fig. 3 (a). Theoretical analysis also supports this experimental result that four wave mixing suppresses S_2 generation at high pressures.

In D_2, the residual pump energy decreases gradually, up to a pressure of 45 atm. This is typical, because of the small Raman gain coefficient of D_2. A steadily rising trend is observed in S_2 rather than suppression, reflecting that a smaller optical dispersion effect exists in D_2 than in H_2 and CH_4. At 45 atm, the measured S_0, S_1 and S_2 conversion efficiencies are 25, 26 and 23% respectively which gives a rather uniform energy distribution.

The increase of S_0 with pressure in CH_4 above 7 atm is an outstanding feature, indicating that the Raman gain is decreasing with pressure. Another characteristic is that the energy conversion to S_1 dominated other SRS

components and was as high as 40% at 20 atm. S_2 appears notable only in a narrow range around 7 atm. The low pressure shift of the second Stokes maximum and its fast depletion compared to H_2 shows that the optical dispersion in methane is the most serious among the three gases.

In conclusion, we have investigated the performance of a single-pass SRS system, using hydrogen, deuterium and methane gases as Raman media. Results indicates that among the three gases, CH_4 transfers very little energy to higher order Stokes and anti-Stokes radiation, and most of the energy is found in the residual pump and first Stokes, at high cell pressure. Thus it is appropriate for generating first Stokes but not suitable for multiwavelength purposes. For H_2 and D_2, pump energy is fairly well distributed in fundamental, first, and second Stokes. Keeping the hydrogen pressure in the range of 10-20 atm and deuterium above 40 atm, multiwavelength output can be generated with reasonable energy per pulse for aerosol lidar applications.

References

[1]. R.M. Measures, Laser remote sensing, (John Wiley & Sons, New York,1984).

[2]. N. Sugimoto, Y.Sasano, H. Nakane, S.Hayashida-Amano, I.Matsui, A.Minato, Conference on Laser and Electro-optics, Baltimore, MD, April 20-24, 1989.

[3]. D. C. Hanna, D. J. Pointer and D. J. Pratt, IEEE J. Quantum Electron., QE-22 (1986) 332.

[4]. R. Mahon, T.J. McIlrath, V. P. Myerscough, and D. W. Koopman, IEEE J. Quantum Electron., QE-15 (1979) 444.

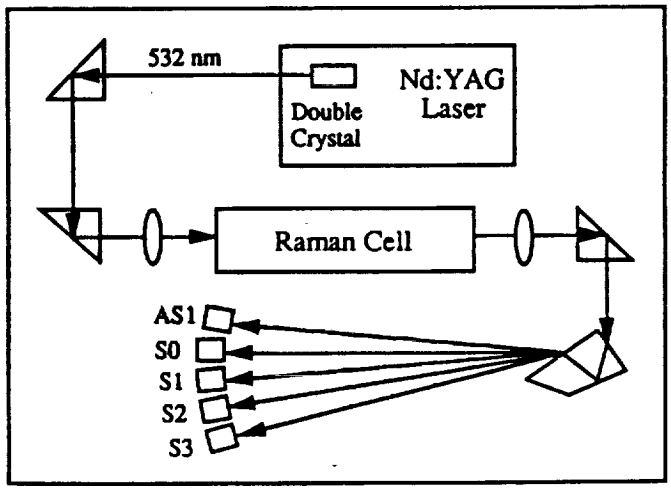

Figure 1. Experimental set-up.

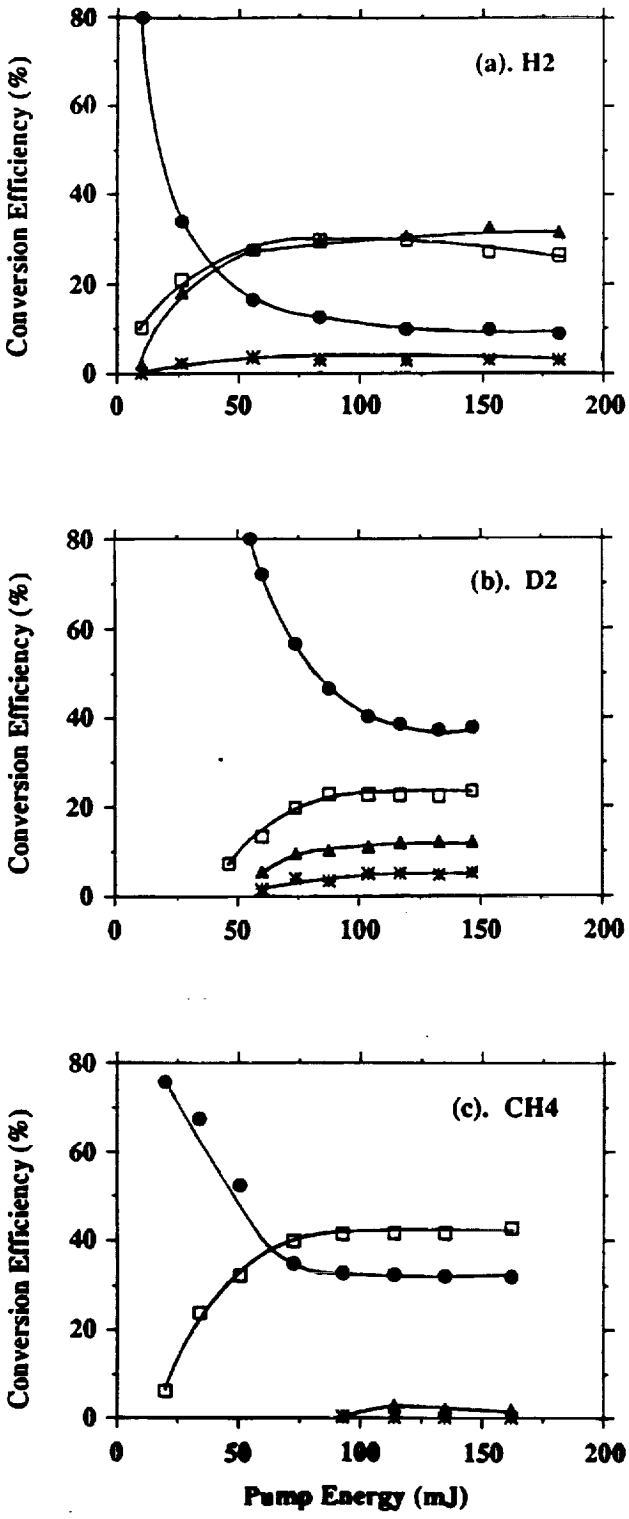

Figure 2. Conversion efficiency of pump energy to fundamental (●), first Stokes (□), second Stokes (▲) and first anti-Stokes (*) as a function of pump eneergy at pressure of 20 atm in (a) H_2, (b) D_2, (c) CH_4.

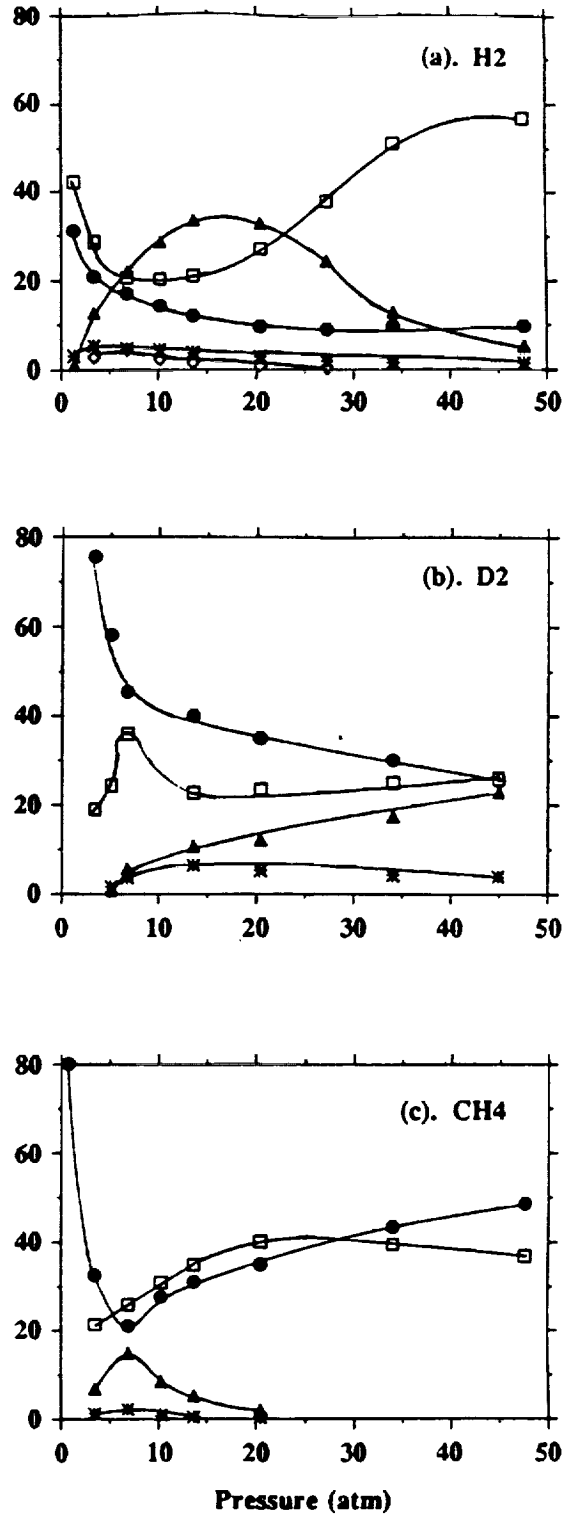

Figure 3. Energy Conversion efficiency to fundamental (●), first Stokes (□), second Stokes (▲), first anti-Stokes (*) and third Stokes (◇) as a function of gas pressure at pump energy of 150 mJ in (a) H_2, (b) D_2, (c) CH_4.

APPENDIX C

MULTIPLE WAVELENGTH GENERATION IN MOLECULAR GASES FOR LIDAR APPLICATIONS

ZHIPING CHU, UPENDRA N. SINGH, and THOMAS D. WILKERSON

University of Maryland
Institute for Physical Science and Technology
College Park, Maryland 20742-2431
Tel: (301) 405-4851, (301) 405-4850
Fax: (301) 314-9363

Submitted to Applied Optics, Aug. 1990

Abstract

We report experimental results of multiple Stokes generation of a frequency-doubled Nd:YAG laser in H_2, D_2 and CH_4 in a focusing geometry. The energies at four Stokes orders were measured as functions of pump energy and gas pressure. The characteristics of the Stokes radiation generated in these gases are compared for optical production of multiple wavelengths. The competition between Raman components is analyzed in terms of cascade Raman scattering and four–wave mixing. The results indicate the possibility of using these generation processes for atmospheric aerosol measurements by means of multiwavelength lidar systems. Also the results distinguish between the gases, as regards the tendency to produce several wavelengths (H_2, D_2) *versus* the preference to produce mainly first Stokes radiation (CH_4).

Key words

Stimulated Raman scattering, Multiwavelength generation, Aerosol lidar application, Lidar, Raman-shifting in molecular gases.

I. Introduction

The atmosphere contains particles whose sizes span many orders of magnitude. Since the scattering properties of aerosols are strongly dependent on the wavelength of the illuminating light,[1] quantitative scattering measurements of aerosol type and size distributions requires the availability of light in different wavelength ranges with adequate energy.[2] For this purpose Raman scattered radiation is attractive because of the potential for multiple Stokes shifts which can produce radiation over a considerable wavelength range and with a reasonable energy conversion.

A series of experiments has been done on the generation of Stokes orders using a frequency-doubled Nd:YAG pump laser at 532 nm in hydrogen, deuterium and methane and using a focused geometry. In addition to stimulated Raman scattering (SRS), four–wave mixing processes also generate light at the Stokes frequencies. A detailed investigation of the processes under a variety of conditions is necessary if a reasonably uniform distribution of energy among the Stokes components is required. In this paper, we report on the results of a study of multiple wavelength generation and the optimization techniques employed. We discuss the similarities and differences between the Stokes orders generated in the different molecular gases. We also analyze the characteristics of the multiple Stokes generation in considering the relative importance of the stimulated Raman and the four–wave mixing effects.

II. Experiment

A schematic of the experiment used for studying the properties of forward Stokes generation is shown in Fig. 1. The pump light is the output of a frequency doubled Nd:YAG laser at 532 nm, linearly polarized, with pulse width of 10 nsec, beam diameter of 6 mm, divergence of 0.6 mrad and repetition rate of 10 Hz. The

Raman cell was a 1 meter long, single-pass gas cell in which we varied the gas pressure up to 45 atm. Lens L_1 before the cell was used to control the confocal parameter of the pump laser beam. L_2 at the exit of the cell collimated the output beam from the Raman cell. A Pellin-Broca prism at the exit of the Raman cell separated the output into different Stokes orders which were monitored by means of energy meters. We measured the incident pump energy, the transmitted pump energy S_0, first Stokes energy S_1, second Stokes energy S_2, and first anti-Stokes energy AS_1. Third Stokes energy S_3 was measured only in H_2. Higher order Stokes components were too weak for ordinary lidar applications and were neglected in this study.

Three optimization techniques were used in this experiment for controlling the stimulated Raman outputs. The first was to vary the pump beam energy over the range of 0 – 200 mJ; the second was to vary the gas pressure from 0 to 45 atm; the third was to control the pump power density at the center of the cell by varying the confocal parameter of the focused pump beam.

III. Raman Gain and Wave-Vector Mismatch Calculations

When a gas cell at low pressure is pumped by a high intensity laser, both stimulated Raman and four-wave mixing processes will happen. The first Stokes radiation is produced by SRS. Since second Stokes may be produced by either four-wave mixing of the original pump and the generated Stokes, or cascade SRS excitation (the first Stokes radiation is strong enough to pump the second Stokes generation directly), it is important to identify the source of the second Stokes in the experiment. In this section some related parameters are calculated for the purpose of data analysis.

A. Raman Gain Coefficient Calculation

For gases, the plane wave, steady-state Raman gain coefficient g_R can be calculated from:[3]

$$g_R = \frac{2\lambda_s^2}{hc\upsilon_s} \frac{\Delta N}{\pi c \Delta\upsilon_s} \left(\frac{d\sigma}{d\Omega}\right) \quad (1)$$

where λ_S is the Stokes wavelength in cm, υ_S is the Stokes frequency in cm^{-1}, c is the speed of light in cm/sec, h is Planck's constant 6.626×10^{-34} J sec, ΔN is the difference in population between the initial and final states in cm^{-3}, $\Delta\upsilon_S$ is the Raman linewidth (FWHM) in cm^{-1}, and $d\sigma/d\Omega$ is the differential cross section for Raman scattering in cm^2/sr.

The Raman gain coefficient g_R is calculated for H_2, D_2 and CH_4. The parameters used for the Raman gain calculation are listed in Table I. The wavelengths for the principal Stokes and anti-Stokes radiations are also given. The values used for ΔN, $\Delta\upsilon_S$ and $d\sigma/d\Omega$ are essentially the same as those used by Hanna *et al.*,[4] except that a more general formula is used for $\Delta\upsilon_S$ in the case of hydrogen,[5] and the most recently published data have been used for deuterium.[6] Clearly the Raman gain in Table I is much greater for H_2 than for D_2 and CH_4.

The pressure dependence of the Raman gain can be seen clearly from the simplified form of Eq. (1):

$$g_R = A\, p / \Delta\upsilon_S \quad (2)$$

where A is a constant dependent on the molecular medium. From substitution of $\Delta\upsilon_S$ (see Table I) for H_2 , D_2 and CH_4, Fig. 2 shows the calculated Raman gain coefficients of three gases at different pressures. At low pressures, g_R increases at different rates for different gases, where the rate for D_2 is the greatest and for CH_4 is the smallest. At high pressures, g_R becomes saturated, the gain being the highest for

H_2 and the lowest for D_2. Both gain curves are essentially flat for p greater than 20 atm, but the gain for CH_4 is still increasing even at 100 atm. The pressure dependence of the Raman gain indicates that Raman effect does limit the second Stokes generation at low pressure, because of the finite Raman gain, but does not suppress the second Stokes in the high pressure region.

B. Wave-Vector Mismatch Calculation

For four–wave mixing, if we neglect the higher order Stokes contributions to second Stokes production and only consider the pump, first Stokes and first anti-Stokes, the mixing process can be either type I or type II:

$$\text{I:} \quad \omega_{S2} = \omega_{S0} + \omega_{S1} - \omega_{AS1} \tag{3-a}$$

$$\text{II:} \quad \omega_{S2} = 2\omega_{S1} - \omega_{S0} \tag{3-b}$$

For a cell which is very long compared to the laser confocal parameter, assuming that only a lowest order Gaussian beam is produced, the second Stokes power, P, generated by four–wave mixing is given by[8]

$$P = B\, p^2 \exp(-b|\Delta k|) \tag{4}$$

where B is a constant, independent of pressure, b is the laser confocal parameter in cm and Δk is the wave vector mismatch caused by the dispersion of the medium; i. e.,

$$\text{I:} \quad \Delta k = k_{S2} - (k_{S0} + k_{S1} - k_{AS1}) \tag{5-a}$$

$$\text{II:} \quad \Delta k = k_{S2} - (2k_{S1} - k_{S0}), \tag{5-b}$$

where $k_i = 2\pi n_i / \lambda_i$ is the wave vector for the ith order Raman component and n_i is refractive index which is proportional[9] to p. The empirical refractive index formula at wavelength λ is used here to estimate the pressure effect,[10]

$$n = \frac{10^{-6}\, p\, r}{1 + \frac{T}{273}} + 1 \tag{6}$$

where T is temperature in ^{0}C, p is pressure in atm, and r is an optical dispersion parameter related to the refractive index at the pressure of 1 atm and temperature of 0 ^{0}C, and is defined as,[10,11]

$$r = 10^6 (n_{0^0C,\,1\,atm} - 1) \tag{7-a}$$

$$\left[\frac{3}{2}\frac{n^2_{0^0C,\,1\,atm} - 1}{n^2_{0^0C,\,1\,atm} + 2}\right] = \frac{a_1}{a_4 - \lambda^{-2}} + \frac{a_2}{a_5 - \lambda^{-2}} + \frac{a_3}{a_6 - \lambda^{-2}} \tag{7-b}$$

where a_1, a_2, a_3, a_4, a_5 and a_6 are constants,[11] and λ is wavelength in cm. Inserting Eqs (5) and (6) into Eq. (4), we can write the wave vector mismatch and second Stokes power as

$$b\,|\Delta k| = C\,p \tag{8-a}$$

$$P = B\,p^2 \exp(-C\,p) \tag{8-b}$$

where C is a constant. Equation (8) shows that the wave vector mismatch is proportional to pressure. In this model, by using dP/dp=0 one can infer a maximum conversion to S_2 at some intermediate pressure p*

$$p^* = 2 / C. \tag{9}$$

From Eqs. (4), (5), and (6) we can calculate C and p* for type I and type II,

$$\text{I:} \quad C = \frac{2\pi b\, 10^{-6}}{1 + \frac{T}{273}} \left(\frac{r_{S_2}}{\lambda_{S_2}} - \frac{r_{S_0}}{\lambda_{S_0}} - \frac{r_{S_1}}{\lambda_{S_1}} + \frac{r_{AS_1}}{\lambda_{AS_1}}\right) \tag{10-a}$$

$$\text{II:} \quad C = \frac{2\pi b\, 10^{-6}}{1 + \frac{T}{273}} \left(\frac{r_{S_2}}{\lambda_{S_2}} - \frac{2r_{S_1}}{\lambda_{S_1}} + \frac{r_{S_0}}{\lambda_{S_0}}\right) \tag{10-b}$$

$$\text{I:} \quad p^* = \frac{10^6}{\pi b}\left(1 + \frac{T}{273}\right)\left(\frac{r_{S_2}}{\lambda_{S_2}} - \frac{r_{S_0}}{\lambda_{S_0}} - \frac{r_{S_1}}{\lambda_{S_1}} + \frac{r_{AS_1}}{\lambda_{AS_1}}\right)^{-1} \tag{11-a}$$

$$\text{II:} \quad p^* = \frac{10^6}{\pi b}\left(1 + \frac{T}{273}\right)\left(\frac{r_{S_2}}{\lambda_{S_2}} - \frac{2r_{S_1}}{\lambda_{S_1}} + \frac{r_{S_0}}{\lambda_{S_0}}\right)^{-1} \tag{11-b}$$

where all wavelengths (at AS_1, S_0, S_1 and S_2) are given in cm. Inserting the wavelengths in Table I, T=25 ^{0}C and b=3.76 cm (f_{L1} = 1 m) into Eq. (11), the optimization pressures and wave vector mismatches for types I and II in H_2, D_2 and CH_4 are calculated and listed in Table II. The optical dispersion quantity r is also given. Figure 3 shows the calculated wave vector mismatches of type II for three gases at different pressures, indicating the greatest Δk for CH_4 among the three gases.

Table II shows a common feature for three gases: type II four-wave mixing has a smaller wave vector mismatch than type I. From Eq. (4) we can infer that type II is the dominant mixing process in the second Stokes generation.

From the above Raman gain and wave vector mismatch calculations, we can conclude that four-wave mixing dominates the second Stokes generation at low pressures where the wave vector mismatch is small; the SRS contributes more as the gas pressure is increased and the contribution by four-wave mixing decreases.

IV. Experimental Results and Discussion

A. Stokes Orders *versus* Pump Energy

Figure 4 shows the output energies plotted against the pump energy and presented in terms of the conversion efficiency of the pump laser to S_0, S_1, S_2 and AS_1 at pressure of 20 atm. The energy distributions among the Raman orders are quite different for the different gases.

The greatest depletion of the pump energy occurs in H_2 (Fig. 4(a)) corresponding to its having the highest Raman gain (Fig. 2, Table I). When the pump energy was above 100 mJ, the transmitted pump energy S_0 was 10% or less and had a variation of only about 1% over a pump energy range of 100–200 mJ. Once the Raman effect produced S_1, S_2 followed rapidly. S_2 was as strong as S_1 when the pump energy was about 50 mJ and even exceeded S_1 at higher pump energies. This

was an important characteristic for H_2 compared to D_2 and CH_4. In the cascade Raman process, when first Stokes radiation is generated by SRS, more pump energy is needed to generate the second Stokes in cascade. The second Stokes generated in this way can never rise simultaneously with or exceed the first Stokes. In Fig. 4(a) the simultaneous generation and the nearly equal energy distribution of the first Stokes and second Stokes in the whole pump energy range indicates that a dominant contribution to the generation of second Stokes came from four–wave mixing. The anti-Stokes conversion (AS_1) was only 3%, i. e., about one order lower than S_1 and S_2.

Results of similar measurements for D_2 and CH_4 are shown in Figs. 4(b) and 4(c). In the saturation region there was about 5% more pump depletion in CH_4 than in D_2, which was consistent with the higher gain of methane (Table I). In D_2, one characteristic was the more even distribution of energy among S_0, S_1, S_2 and AS_1. In the pump energy range of 150 mJ, the transmitted pump energy was not strongly depleted. In the saturation region, S_0 was 38%, S_1 was 22%, S_2 was 12% and AS_1 was 5%. The anti-Stokes conversion in D_2 was comparable with that in H_2. In the case of CH_4, almost all of the scattered photons were converted to S_1, and S_2 is near zero. S_1 exceeded S_0 at the pump energy of 65 mJ and saturated around 40%. This reflected the fact that four–wave mixing was not prominent with CH_4 (in contrast to D_2) at 20 atm gas pressure, which agreed with the calculation of the greatest wave vector mismatch of CH_4 indicated in Table II and Fig. 3.

From Fig. 4 we see that there is one common feature for the Stokes generation processes in the three gases: once saturation is reached, the conversion efficiency ratios of the various Stokes components remain roughly fixed as the pump laser power is varied.

B. Pressure Effect in Multiple Stokes Generation

We investigated multiple Stokes generation by operating at the highest

pressure possible. Figure 5 shows the variations of conversion efficiency with gas pressure in H_2, D_2 and CH_4.

We first discuss the results for H_2 (Fig. 5(a)). One feature is the relative constancy of the transmitted pump energy S_0 at high pressures. This energy varied by about 1% in the pressure range 20–50 atm, indicating that the Raman gain was constant above 20 atm and the depleted photons were shifted into different Stokes orders. The second feature is a minimum conversion to first Stokes radiation around 10 atm. We observed that a more favorable S_1 conversion occurred at pressures below 5 atm or above 30 atm. In contrast to S_1, there was a maximum in S_2 around 13 atm, and it dominated the Stokes conversion processes at that pressure. Our experimental result (p^*_{exp} = 13 atm) is closer to that of type II four-wave mixing (Table II) and agrees with the prior measurements by Loree *et al.*,[12] which showed that the number of observed Raman lines was the greatest for p ~ 10 atm. The intensity distribution of the second Stokes was observed to evolve from the Gaussian structure to a circular ring pattern, and the ring diameter increased with pressure.

The third Stokes S_3 at 1.563 μm was also generated in H_2 at low pressures, as shown in Figure 5(a). The energy in the third order Stokes was comparable to that in the anti–Stokes. S_3 decreased with pressure from 7.5 atm and upward, confirming that the high pressure drop in second Stokes energy was not caused by the third Stokes generation through cascade Raman process, but rather by four-wave mixing.

The experimental results in Fig. 5(a) also show that for optimizing just the S_1 output in H_2, increasing the pressure to above 30 atm or decreasing the pressure to below 5 atm are good choices, but for maximizing the *number* of wavelengths having reasonable energies for lidar use, pressures in the range 5–15 atm are the most suitable. In consideration of the equal beam divergence requirement in lidar applications[13], the operating pressure should be chosen as low as possible in the above

range because of the second Stokes ring pattern.

Fig. 5(b) shows the variation of S_n with pressure in D_2. The remaining pump energy steadily decreased over the pressure range 10 - 45 atm. This was identical with the smaller Raman gain coefficient of D_2. A peak value of 36% energy conversion to S_1 occurred at 7 atm; S_1 efficiency decreased at the expense of conversion to S_2 as pressure was increased from 7 to 15 atm, and then increased somewhat because of the SRS transfer from pump light as pressure was higher than 15 atm. It is noteworthy that S_2 increases steadily rather than dropping in the pressure range of 45 atm, which is consistent with its smallest Δk and highest p^* in the theoretical prediction of Table II. *At 45 atm, the measured S_0, S_1 and S_2 conversion efficiencies were 25, 26 and 23% respectively, providing a relative uniform distribution of optical energy over these wavelengths.*

Instead of the progressive pump depletion with increasing pressure in H_2 and D_2, the increase of S_0 with pressure in CH_4 when the pressure was above 7 atm was one notable characteristic. S_1 was as high as 40% at 20 atm pressure, and dropped at higher pressure. S_2 appeared noticeably only in a narrow range around 7 atm, and its maximum of 15% coincided with the minimum of S_0, which agrees with its lowest p^* among the three gases as predicted in Table II. The decrease in Raman conversion at high pressure in CH_4 may be due to the competition from other nonlinear processes, such as stimulated Brillouin scattering.

The measured optimization pressures in these gases are all higher than the theoretical predictions. The discrepancy may be due to the interaction of four-wave mixing and cascade Raman scattering. Another possible reason for the discrepancy is the assumption of a single Gaussian mode made on Eq. (4). In general the wave generated by four-wave mixing has a multimode structure which will shift the optimization pressure to the higher side.[8]

In all three cases, indicated in Fig. 5, the anti-Stokes conversion was very low, and it peaked at low gas pressure. This is caused by four-wave mixing effects, which

are denoted here by types III and IV.

$$\text{III:} \quad \omega_{AS1} = \omega_{S0} + \omega_{S1} - \omega_{S2} \tag{12-a}$$

$$\text{IV:} \quad \omega_{AS1} = 2\omega_{S0} - \omega_{S1} \tag{12-b}$$

Equations (12) and (3) belong to the same general type of four-wave mixing. Equation (6) can then be used to estimate the pressure effect of anti-Stokes generation, which manifests a high pressure suppression effect similar to that of S_2. Table III lists the wave vector mismatch and peak pressures calculated for the anti-Stokes processes. The measured maximum conversion efficiencies for anti-Stokes radiation are 5.5% at 3.5 atm (H_2), 6.5% at 13.5 atm (D_2) and 2.2% at 6.8 atm (CH_4). Comparing Table II and Table III, we see that the discrepancies between the calculations and experiments for anti-Stokes are smaller than those for second Stokes. We also see that the wave vector mismatch of type II for anti-Stokes is larger than that for second Stokes.

In order to achieve the high power density required by Stokes generation, we used lenses of different focal length (50, 75, 100, 150, 200 cm) at different cell pressures. When the lens focal length was greater than 100 cm, the power densities at the input and output windows exceeded the damage threshold. Thus we only used lenses having focal lengths less than 100 cm. Focusing dramatically altered the energy distribution between the Raman orders. The result of one such investigation is shown in Fig. 6, where lenses of focal length f_{L1} = 100 cm and f_{L1} = 50 cm were used with D_2 for a range of cell pressures. The 50 cm focal length gave the lower Raman conversion. In the case of very tight focusing (50 cm), we found that the total of the four Raman components deviated greatly from 100% at high pressure; this loss was proportional to the pump energy. This energy loss may have been caused by competing nonlinear processes arising from the higher local density of pump light near the focus[14] and the simultaneous generation of higher order Raman components by four-wave mixing.

V. Conclusions

We have investigated the performance of a single-pass, multi-order Stokes generation system using hydrogen, deuterium and methane gases as Raman media. Among the three gases, CH_4 transfers very little energy to high order Stokes and anti-Stokes outputs; most of the energy is concentrated in the pump and first Stokes, especially at high pressures. Thus CH_4 is appropriate for generating first Stokes light, but not for multiple wavelength applications. For H_2 and D_2, energy is distributed over second Stokes as well as the first Stokes and the transmitted pump. Varying the hydrogen pressure in the range of 5 to 15 atm, and deuterium above 40 atm, is a suitable method for simultaneous generation of a variety of wavelengths with reasonable energy for lidar applications. D_2 is a suitable gas for producing radiation on the shorter wavelength side, and the optimum pressure for this is about 13 atm.

Acknowledgement

The authors would like to thank B. Bloomer and G. Treacy for their excellent technical assistance, R. Mahon and X. Xiong for helpful discussions and comments on the manuscript.

References

1. R. M. Measures, Laser remote sensing, John Wiley & Sons, New York, 1984.
2. Y. Sasano and E. V. Browell, "Light Scattering Characteristics of Various Aerosol Types Derived from Multiple Wavelength Lidar Observations," Appl. Opt. **28**, 1670-1679 (1989).
3. John J. Ottusch and David A. Rockwell, "Measurement of Raman Gain Coefficient of Hydrogen, Deuterium, and Methane," IEEE J. Quantum Electron. **QE-24**, 2076-2080 (1988).
4. D. C. Hanna, D. J. Pointer and D. J. Pratt, "Stimulated Raman Scattering of Picosecond Light in Hydrogen, Deuterium, and Methane," IEEE J. Quantum Electron. **QE-22**, 332-336 (1986).
5. W. K. Bischel and M. J. Dyer, "Wavelength Dependence of the Absolute Raman Gain Coefficient for the Q(1) Transition in H_2," J. Opt. Soc. Amer. B **3**, 677-682 (1986).
6. D. A. Russell and W. B. Roh, "High-Resolution CARS Measurement of Raman Linewidths of Deuterium", J. Mol. Spectrosc. **124**, 240-242 (1987).
7. N. Bloembergen, G. Bret, P. Lallemand, A. Pine and P. Simova, "Controlled Stimulated Raman Amplification and Oscillation in Hydrogen Gas," IEEE J. Quantum Electron. **QE-3**, 197-201 (1967).
8. G. C. Bjorklund, "Effects of Focusing on Third-Order Nonlinear Processes in Isotropic Media," IEEE J. Quantum Electron. **QE-11**, 287-296 (1975).
9. R. Mahon, T. J. McIlrath, V. P. Myerscough, and D. W. Koopman, "Third-Harmonic Generation in Argon, Krypton, and Xenon: Bandwidth Limitations in the Vicinity of Lyman-α," IEEE J. Quantum Electron. **QE-15**, 444-451 (1979).
10. E. W. Washburn, International Critical Tables, McGraw - Hill, New York, vol. VII, **2-11**, 1930.
11. J. Bartels, H. Borchers, H. Hausen, K. -H. Hellwege, K L. Schafer and E. Schmidt,

Landolt - Bornstein Zahlenwerte und Funktionen, Berlin Gottingen Heidelberg, Springer-Verlag, 6.871 – 6.885, 1962.

12. T. R. Loree, R. C. Sze, D. L. Barker, and P. B. Sccott, "New Lines in the UV: SRS of Excimer Laser Wavelengths," IEEE J. Quantum Electron. **QE-15**, 337-342 (1979).

13. D. Diebel M. Bristow, and R. Zimmermann, "Stokes Shifted Laser in KrF-Pumped Hydrogen: Reduction of Beam Divergence by Addition of Helium," submitted to Appl. Opt. 1990.

14. Z. Chu, U. N. Singh, T. D. Wilkerson, "A Self-Seeded SRS System for the Generation of 1.54 μm Eye-Safe Radiation," Opt. Commun. **75**, 173-178 (1990).

FIGURE CAPTIONS

Figure 1. Experimental setup for the multiple Stokes generation.

Figure 2. Calculated Raman Gain Coefficient g_R as a function of gas pressure for H_2, D_2 and CH_4.

Figure 3. Calculated wave vector mismatch Δk as a function of gas pressure for H_2, D_2 and CH_4.

Figure 4. Conversion efficiency of pump energy to transmitted pump (●), first Stokes (□), second Stokes (▲), third Stokes (Δ) and first anti-Stokes (○) as a function of pump energy in H_2 (a), D_2 (b) and CH_4 (c) at pressure of 20 atm.

Figure 5. Energy conversion efficiency as a function of gas pressure to transmitted pump (●), first Stokes (□), second Stokes (▲) and first anti-Stokes (○) in H_2 (a), D_2 (b) and CH_4 (c) for a constant pump energy of 150 mJ.

Figure 6. Conversion efficiency for the Stokes orders is shown as a function of gas pressure for two focusing geometries: transmitted pump with f_{L1}= 50 cm (●); first Stokes with f_{L1}= 50 cm (■); second Stokes with f_{L1}= 50 cm (▲); transmitted pump with f_{L1}= 100 cm (○); first Stokes with f_{L1}= 100 cm (□); second Stokes with f_{L1}= 100 cm (Δ).

TABLE CAPTIONS

Table I. Parameters used for the calculation of the Raman gain at a pressure of 20 atm and temperature of 25 ^{0}C.

Table II. Calculations of optimum pressure and wave vector mismatch for second Stokes at a pressure of 20 atm and temperature of 25 ^{0}C.

Table III. Calculations of optimization pressure and wave vector mismatch for anti-Stokes at a pressure of 20 atm and temperature of 25 ^{0}C.

Gas	$\lambda_{AS1,S0\,(1,2)}$ (nm)	ΔN (cm^{-3})	$\Delta\upsilon_s$ [$10^{-3}cm^{-1}$] & p (atm)	$\frac{d\sigma}{d\Omega}$ [$10^{30}cm^2/sr$]	g_R (cm/GW)
H_2 Q(1) (4155 cm^{-1})	436 532 683 954	0.66 N_{tot}	$\frac{11.2}{p}$ + 1.58 p	0.79	2.72
D_2 Q(2) (2987 cm^{-1})	459 532 633 780	0.38 N_{tot}	$\frac{3.67}{p}$ +3.58 p	0.80	0.56
CH_4 Q (2917 cm^{-1})	461 532 630 771	N_{tot}	320 + 12 p	2.7	0.63

Gas	$\Gamma_{AS1,\,S0\,(1,2)}$	p* (atm)	Δk (cm^{-1})
H_2	145.01 142.98 141.40 140.24	I: 2.26 II: 5.27	I: 4.71 II: 2.02
D_2	108.14 107.43 106.84 106.35	I: 8.47 II: 18.73	I: 1.26 II: 0.57
CH_4	448.42 444.24 440.73 437.88	I: 1.44 II: 3.21	I: 7.37 II: 3.31

Gas	p* (atm)	Δk (cm^{-1})
H_2	III: 2.26 IV: 3.95	III: 4.71 IV: 2.69
D_2	III: 8.47 IV: 15.46	III: 1.26 IV: 0.69
CH_4	III: 1.44 IV: 2.62	III: 7.37 IV: 4.06

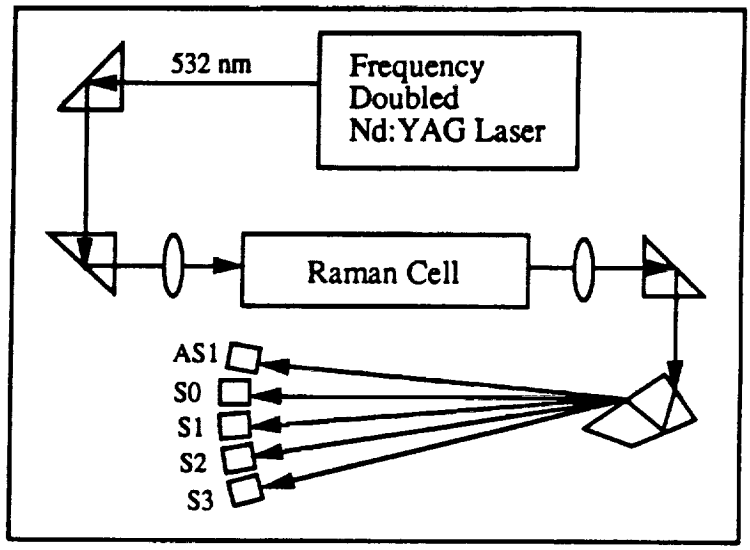

Figure 1

Chu, Singh and Wilkerson

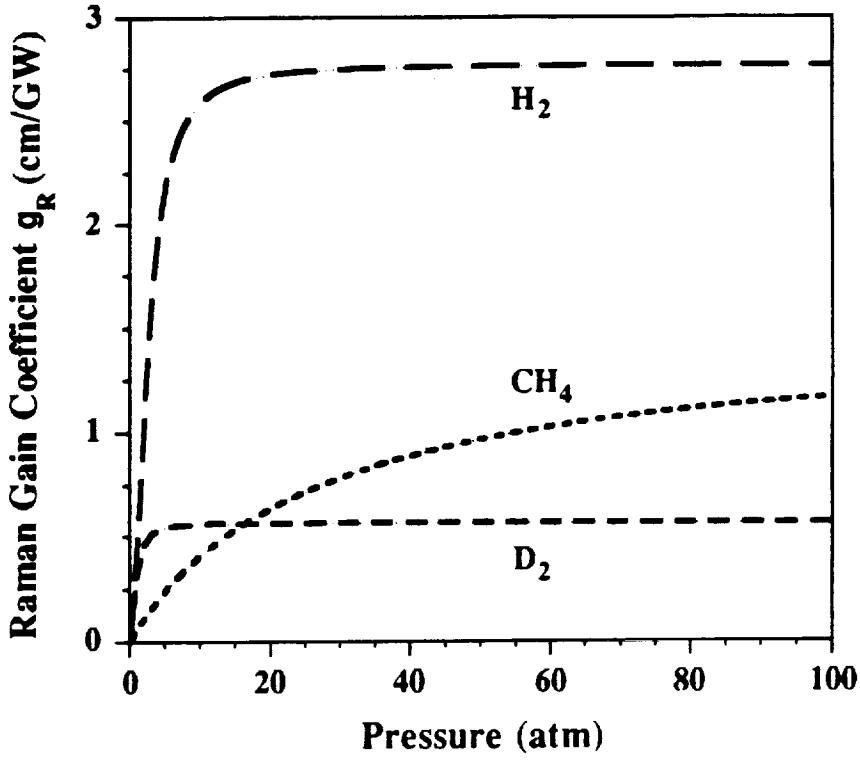

Figure 2.

Chu, Singh, Wilkerson

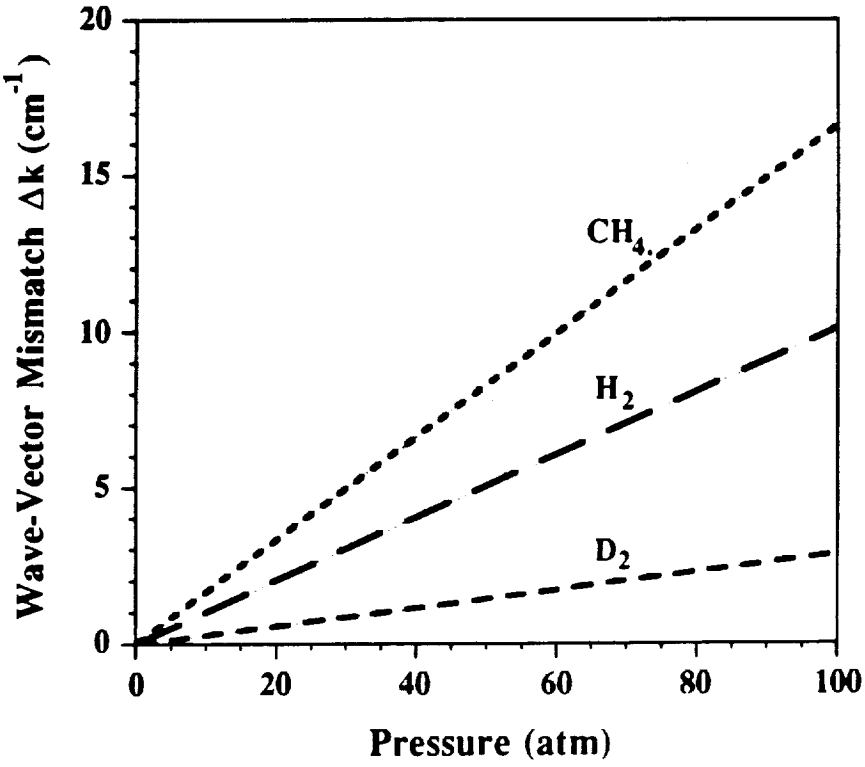

Figure 3.

Chu, Singh, Wilkerson

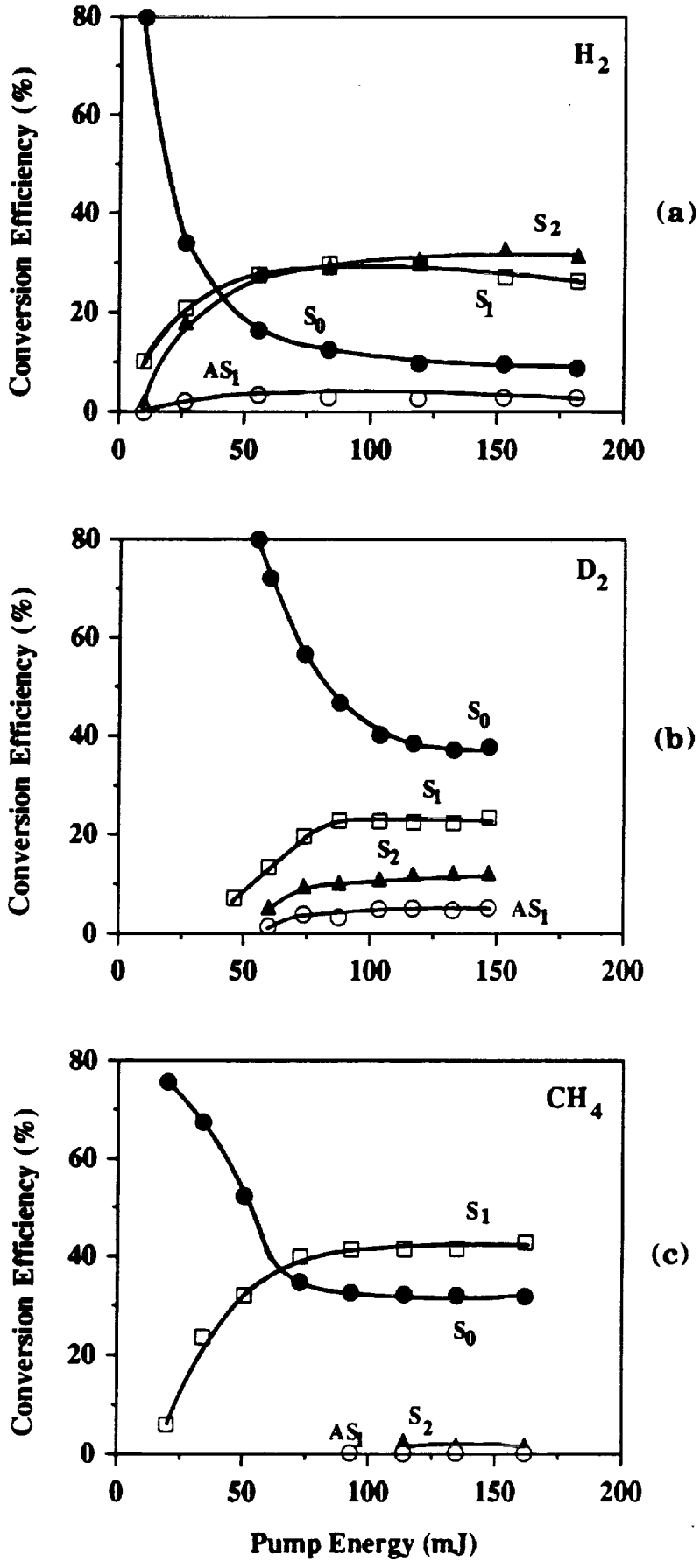

Figure 4.

Chu, Singh, Wilkerson

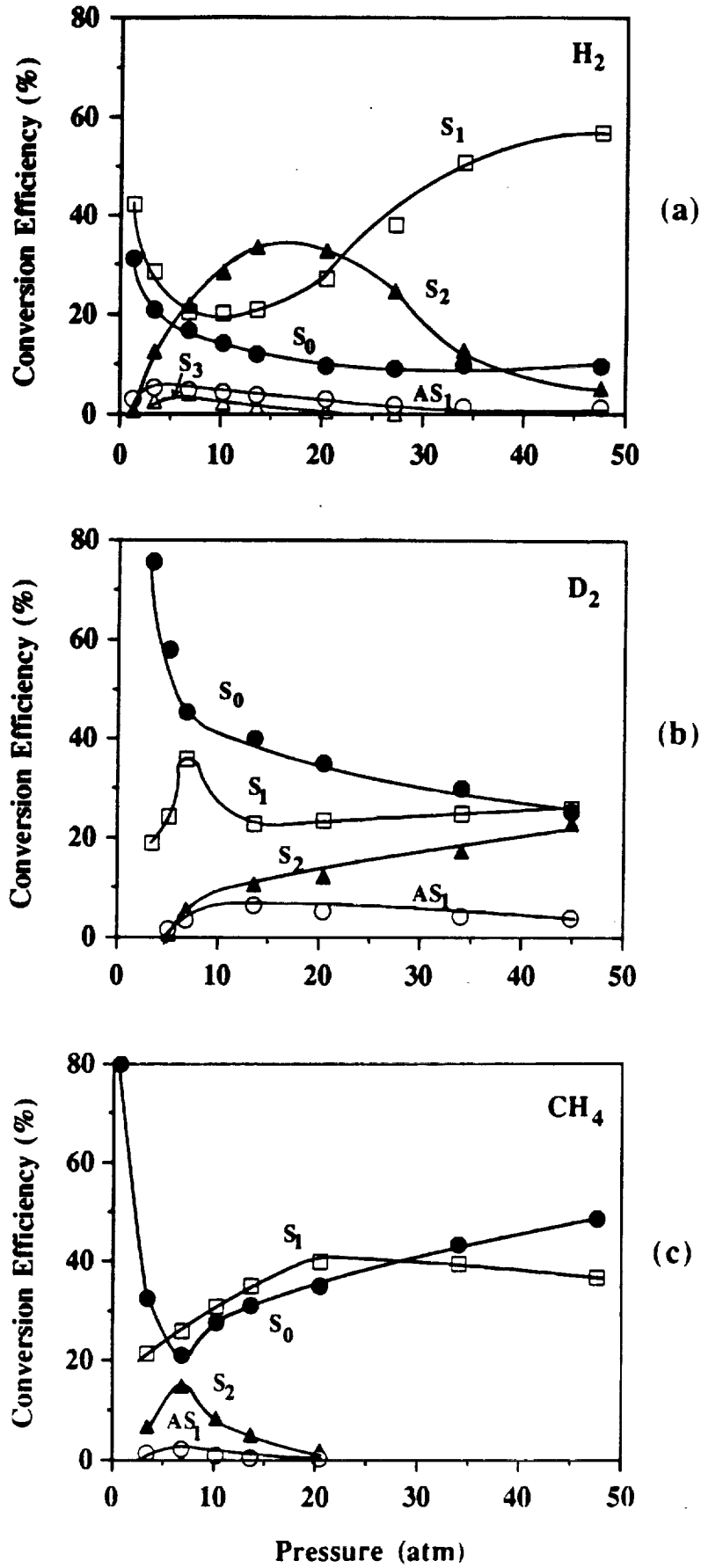

Figure 5.

Chu, Singh, Wilkerson

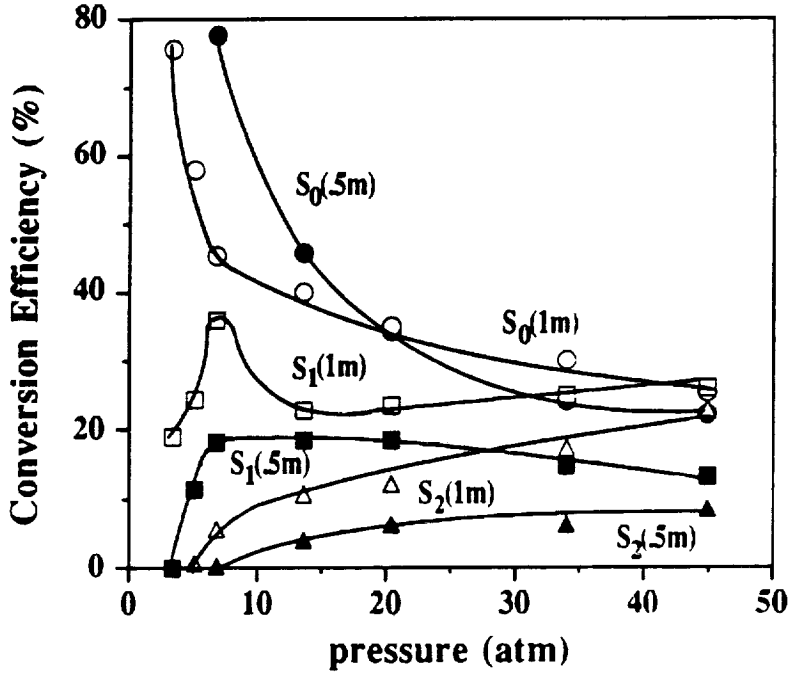

Figure 6.

Chu, Singh, Wilkerson